Results in Physics 19 (2020) 103691

Contents lists available at ScienceDirect

Results in Physics

journal homepage: www.elsevier.com/locate/rinp

Electrical transport during growth, aging and oxidation of copper ultrathin films before percolation

Francisca Marín, Gabriel Gray, Claudio Gonzalez-Fuentes, Valeria del Campo, Patricio Häberle, Ricardo Henríquez *

Departamento de Física, Universidad Técnica Federico Santa María, Av. España 1680, Valparaiso 2390123, Chile

ARTICLE INFO

Keywords:
Electrical transport
Ultrathin films
Copper
Oxidation
Chromium
Tunnel current
Gold

ABSTRACT

The electrical transport mechanism of non-percolated copper ultrathin films was studied. For this purpose, resistance behavior was measured during sample growth, aging in vacuum and oxidation in air, and contrasted with a model based on tunnel current and on film's morphology. In addition, the electrical characterization of chromium and gold ultrathin films was performed and compared with that obtained for copper. All films were grown on muscovite mica through thermal evaporation under high vacuum conditions. Electrical characterization throughout films' growth, aging and oxidation was performed in situ and in real time. Finally, to address the transport mechanism of non-percolated oxidized copper films, samples were put into a cryostat in which electrical resistance was measured changing the temperature between 35 and 300 K. It was found that the three materials present an almost constant resistance decay during growth. This resistance decrease was studied for copper films by fitting a tunnel transport model which considered islands' distance as a function of film thickness, indicating a resistance reduction given by coalescing islands. During aging, the resistance of copper and gold ultrathin films increases without reaching a saturation value after 30 min, with a behavior independent of the material or the initial resistance. The theoretical model applied to copper film resistance explains the increment by further formation of 3D structures, mainly conducted by atom diffusion on the substrate. Finally, a change in the resistance behavior is observed during the oxidation of copper ultrathin films, electrical transport is mediated by two mechanisms a semi-conductor type, resembling that of oxidized chromium layers, and a tunnel conduction type, observed in gold films. The first mechanism dominates when temperature is above 200 K, while tunneling is the main process for temperatures below 150 K.

Introduction

The miniaturization imposed by current information technology has brought the characteristic dimensions of electrical conductors to sizes lower than 10 nm [1–3]. To describe the physics of transport, in these confined conducting channels, additional mechanisms contributing to the electrical resistance must be considered, besides those regularly included in the description of thin films or wires [2,4–6]. These new effects are observed in conductors close to the condition of electrical percolation in 2D structures.

The thickness at which a film reaches electrical percolation depends on its growth mode. In the early stages of Volmer-Weber growth (or 3D growth) of a metallic thin film over an insulating substrate, material is deposited forming small separated structures (similar to islands). As more material arrives, islands grow and coalesce into larger structures. Once a continuous electrical path is established through the structure the percolation is reached. From the electrical resistance viewpoint, the range where percolation is reached is between $\sim 10^6$and $\sim 10^4$ Ω [7,8], mainly controlled by tunnel current [3,9,10]. Even when this limit is reached, the effect of tunnel current is still evident in the conduction's temperature dependence, where a metallic behavior is not yet observed, namely the resistance of the metal does not increase linearly with temperature [3,8,11] in this regime.

Systems in the vicinity of the percolation, also present a morphology with a high relation area-volume. Thus, the behavior of their electrical resistance is highly sensible to changes in their surface, which make them good candidates for sensors applications. For example, the measurement of electrical resistance of a non-percolated gold film has been proposed as sensor of nanoclusters coverage [10]; resistance increase in a bundle of carbon nanotubes decorated with nanoparticles are used as

* Corresponding author.
E-mail address: ricardo.henriquez@usm.cl (R. Henríquez).

https://doi.org/10.1016/j.rinp.2020.103691
Received 22 September 2020; Received in revised form 17 November 2020; Accepted 1 December 2020
Available online 7 December 2020

gas sensors for NO_2, NH_3, H_2S [12], H_2, and C_2H_2 [13]; conductivity of a polyacrylonitrile and carbon black complex shows an high sensitivity to the presence of NO and CO gases [14]; and the electrical response of silica nanospring mat coated with a thin zinc oxide layer has been proposed to detect ammonium nitrate vapor [15]. In all these systems, the percolation of the different components strongly impacts in their detection ability.

On the other hand, one of most used materials in the semiconductor industry to transport electrical current, is copper [1,16,17]. This fact increases the relevance of new experimental and theoretical data, regarding electrical transport in nanometric scale structures. Copper presents a 3D growth mode on most substrates [8], therefore its resistance behavior regarding electrical percolation does follow the model described above. However, there are fewer reports compared to other materials, as gold for example, due to its high chemical reactivity in air, which complicates finding correlations between in situ and *ex situ* characterizations. Regarding the oxidation process, it is known that copper exposed to air in ambient condition is oxidized producing mainly cuprous oxide (Cu_2O) during the first few hours, followed later by the appearance of cupric oxide (CuO) [18–21]. Whereas, the former one is a semiconductor with a bandgap of 2.0 eV, the last one presents a lower bandgap, in the range of 1.21–1.51 eV [19]. Although the effect of the oxidation on copper's electrical transport has been studied and modeled extensively [22–24], its impact on ultrathin films before percolation has not been considered in detail.

This work is an experimental study of the evolution of the electrical resistance of copper ultra-thin films, before percolation is achieved. The resistance change was determined in situ and in real time during the film's growth, considering both aging in vacuum and oxidation in air. For comparison purposes, these experiments were also performed on gold and chromium films. The resistance behavior of the copper films during growth and aging was described with a theoretical model based on tunnel current between nanoscale structures and material distribution on the surface. To identify the conduction mechanisms of the oxidized thin films, resistance vs temperature measurements were performed.

Materials and methods

Copper (99.9999% purity, Alfa Aesar), gold (99.999% purity, Alfa Aesar) and chromium (99.994% purity, MaTeck) were thermally evaporated from tungsten baskets in a High Vacuum System (Turbomolecular and diaphragm pump). The substrate was muscovite mica (SPI, V-1 grade). The effective thickness "t" and deposition rate were measured with quartz microbalances (Inficon, XTM/2), previously calibrated through ellipsometry (homemade with Thorlabs components).

During the evaporation process, the pressure was kept at $\sim 1\times10^{-4}$ Pa. Once the sample fabrication was finished, it was kept under vacuum conditions for 30 to 45 min. During this time, the aging process, pressure decreased to $\sim 5\times10^{-5}$ Pa. Finally, the films oxidation was induced in two steps. First air was admitted, through an inlet valve increasing the pressure from $\sim 1\times10^{-4}$ to $\sim 1\times10^{3}$ Pa, in steps of one order of magnitude every three minutes approximately. After this stage, the valve was completely open, and the vacuum system reached ambient pressure. These oxidation steps were labeled as "low pressure oxidation" and "high pressure oxidation", respectively.

Before evaporation the mica pieces were cleaved and placed into a Sputtering System (Quorum, Q150T ES Plus), where two gold contacts (separated by 4 mm) were deposited to perform the electrical characterization.

All electrical characterizations were performed through the measurement of the sample resistance (computer-controlled picoammeter Keithley 6487). DC currents were applied in alternate directions for 5 s each time in order to minimize temperature induced voltages differences. These measurements were performed in situ during films' growth, aging and oxidation.

Electrical resistance as a function of temperature was measured ex situ. For this analysis, films were removed from the evaporation system and inserted into a cryostat (Air Products), changing the temperature between 35 and 300 K, with thermalization times of 20 min for each collected value. The mean resistance during the last two minutes was reported as the value associated to that temperature. Voltages used in all measurements, were in the range in which they did not change the resistance value.

The morphological characterization of samples and substrate was performed through Atomic Force Microscopy (AFM Omicron VT SPM, in contact and/or non-contact mode). Topographic images were analyzed with WSxM [25] and ImageJ softwares.

Raman spectroscopy measurements (Renishaw in-Via, with a 532 nm laser) were performed to assert the presence of copper oxide, once samples were exposed to ambient conditions.

Theoretical model

In the regime controlled by tunnel current, a good approximation of the distance between islands dependence of the electrical resistance, can be obtained from [10,26,27]:

$$R(d) = R_0 \frac{d^2}{\overline{\varnothing}} e^{1.025\sqrt{(m^*\overline{\varnothing})}d} f\left(\frac{\delta E}{kT}\right) \tag{1}$$

where $\overline{\varnothing}$ represents the average tunnel barrier height; m^*, the effective mass of a tunneling electrons; δE, the activation energy; k, the Boltzmann constant; T, the temperature; R_0, a constant; and f can be obtained by [9]:

$$f\left(\frac{\delta E}{kT}\right) = \frac{\left(1 - e^{(\delta E/kT)}\right)^2}{1 - (1 - e^{(\delta E/kT)})e^{(\delta E/kT)}} \tag{2}$$

To contrast experimental data with this expression, a model for the temporal evolution of separation distance d must be constructed.

This distance was estimated from a series of experimental reports [28,29] in which islands size and number by surface area were determined as a function of deposited material (on the substrate). Fig. 1 shows a representation of a model formed by N islands of radius a, separated by a distance d, homogenously distributed on a substrate of dimension LxL.

From the above considerations, the quotient $\frac{L}{\sqrt{N}}$ is the lateral

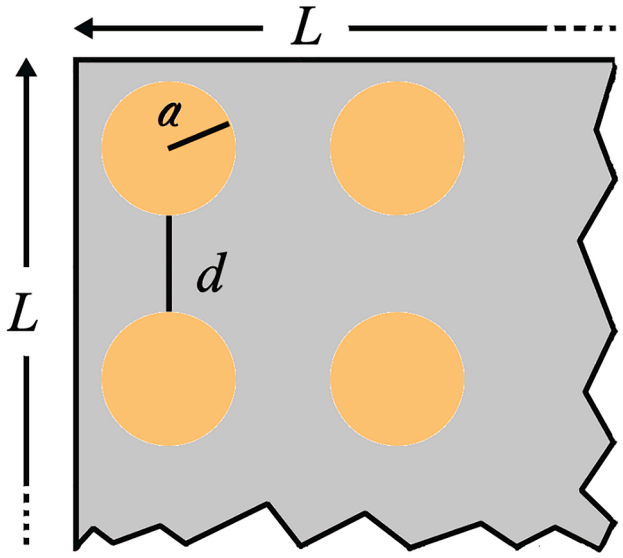

Fig. 1. Schematic representation of islands' radii's a, sample size L^2, and island separations d.

dimension occupied by a single island. Then, d can be estimated from:

$$d = \frac{L}{\sqrt{N}} - 2a \tag{3}$$

The main ideas in this report will be discussed at the light of this model, however, it is worth to note that it can be substantially improved adding a series of considerations and new parameters. For example, changing the shape of islands on the substrate, from round to elliptical [30]; considering an inhomogeneous island distribution [9,31]; or adding additional transport mechanisms, such as coherent tunneling effects [32].

Film resistance was measured during the three different processes occurring in the samples: film growth, aging and oxidation. Equation (1) was used as model for resistance change during samples growth and aging. For this purpose, particular approximations were considered to calculate d in each process (as described below in Sections "Evaporation process" and "Aging process"). Electrical conduction during oxidation was analyzed through the temperature dependence of the resistance as explained in Section "The temperature dependence of the resistance".

Evaporation process

During the evaporation process, islands radius and density, they both change as a function of nominal film thickness (h), as described by following expressions [28]:

$$\langle a \rangle \propto h^{1/z}$$

$$\frac{N}{L^2} \propto e^{-Ah^{2/3}}$$

where z represents the dynamic scaling exponent, the bracket labels the mean value, and A is a constant. The expression for island density N/L^2, represents a process named partial coalescence, which consider the variations of island number due to a coalescence and impingement dynamic.

Replacing these relations in equation (3), the separation between the islands as a function of film thickness is obtained as: $d \propto \left(e^{\frac{A}{2}h^{2/3}} / \sqrt{N_0} \right) - 2a_0 h^{1/z}$, which after redefining the constants, takes the following form:

$$d = C_1 e^{C_3 h^{2/3}} - C_2 h^{1/z} \tag{4}$$

Aging process

The aging process, in high vacuum conditions, consist simply in the rearrangement of the structure of the film. It is then expected that the volume of deposited material remains constant while the physical dimensions of the structures may vary. If the islands are modelled as semi spheres, the quantity $N \times \frac{2\pi R^3}{3} = L^2 h$, can be considered time independent during this process. On the other hand, while aging the number of islands changes with time. This temporal evolution have been approximated by [29]:$N(t) \propto \left(\frac{t}{\ln(t)} \right)^{-3/(3+\alpha)}$, where the exponent α has information about the atomic mechanism involved in the mass transport during aging. Rewriting d as a function of the island density N/L^2 and including its time dependence, the final expression for island separations during aging is given by the following expression, after renormalizing the constants,

$$d(t) = d_0 + D_1 \left(\frac{t}{ln(t)} \right)^{3/[2(3+\alpha)]} - D_1 \cdot D_2 \left(\frac{t}{ln(t)} \right)^{1/(3+\alpha)} \tag{5}$$

The temperature dependence of the resistance.

From equation (2), in the regime controlled by tunnel current, the resistance change as a function of temperature has, at first order, two limits behavior. If $\delta E \gg kT$, the dominant term is $e^{\delta E/(kT)}$, whereas for $\delta E \ll kT$, $e^{\delta E/(3kT)}$ is the relevant factor. Both expressions show a behavior analogous to a thermally activated conduction mechanism (as is the case in semiconductors). Improvements to this model have been suggested, by including the thermal expansion of the substrate, hence, inducing changes in the island separation. This effect has been shown to generate very small changes in the resistance [3,9].

Regardless of the case, the standard description of the resistance's temperature dependence in ultra-thin films before percolation, is performed simply by plotting the film's conductance, 1/R, as a function of 1/(kT) (or often 1000/(kT)). These plots simplify the comparison of different behaviors, where the slope is then associated to an activation energy δE.

Results and discussion

Copper is highly reactive in presence of air, therefore other two materials were studied to compare the behavior of the electrical resistance. The first one was gold, which has a similar growth mode to copper and does not show oxidation under atmospheric conditions [8]. The other one was chromium, which is fairly reactive in the presence of air, but nonetheless, the evolution of film growth is quite different to gold and copper [3].

Copper, gold and chromium films were evaporated onto a mica substrate at RT. Evaporation rates were 0.9, 0.9, and 0.6 nm/min, for copper, gold and chromium, respectively. These rate values are lower than those that can substantially modify the morphology of the copper and gold films [8]. Fig. 2 shows the thickness dependence of the resistance for copper, gold and chromium films. As explained above, our purpose is to describe the electronic transport in thin films, before they form continuous conducting channels. In order to assert that percolation has not been reached, only samples that presented resistances higher than $\sim 5 \times 10^6$ Ω once evaporation was finished, were analyzed.

Results show two resistance trends in all samples. First, resistance values oscillate around $\sim 5 \times 10^{10}\Omega$, pointing out that the real sample resistance is higher than the upper limit sensitivity of the equipment. In the second zone, all samples display an almost linear decrease of the resistance as a function of thickness.

Similar resistance values have been reported for a 2.5 nm thick Cu film deposited on glass [32], and ~5 nm thick films evaporated on sapphire [33]. This similarity between copper films on different substrates, contrasts with the poor reproducibility showed for gold samples (see Fig. 1). Also, the thickness dependence of the resistance in these two systems [32,33] present an almost linear behavior, similar to that of our copper samples. Regarding the reproducibility of the resistance, copper samples display a smaller spread in resistance as a function of thickness when compared to gold. A reasonable way to characterize this fluctuation is by quoting the thickness range for a fixed resistance value. For copper a resistance value of $\sim 10^7\Omega$ is reached when the films are within 3 and 5 nm thick.

Also, from Fig. 2, it is clear that chromium films display a completely different behavior. The resistance of all samples decay with a single slope and they also display a high reproducibility (the $10^7\Omega$ limit is reached for films of ~0.5 nm). This performance indicates why Cr is an efficient surfactant layer, that has been used to improve the electronic transport in ultra-thin layers [3,34] grown on different substrates.

To get a deeper understanding of the thickness dependence of copper films' resistance, the parameters for the model described in Section "Theoretical model" were adjusted. As a first approximation, the temperature was considered constant during all the evaporation process, therefore in Equation (1), the product $\frac{R_0}{\varnothing} f\left(\frac{\delta E}{kT}\right)$ can be replaced by a

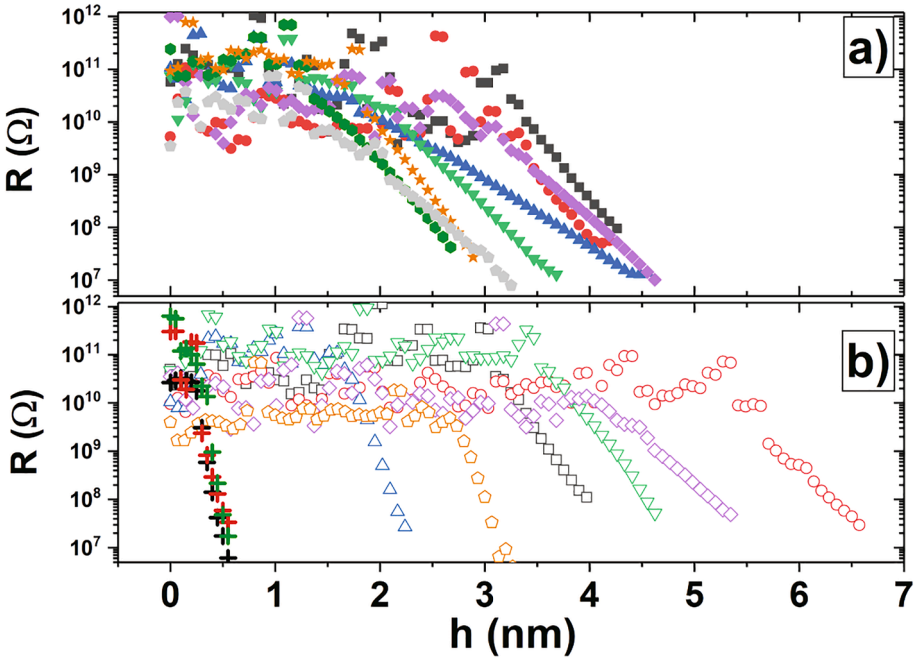

Fig. 2. Thickness dependence of resistance during the evaporation of a) copper films (filled symbols), b) chromium (crosses) and gold films (hollow symbols) on mica at RT.

single constant. Then, by introducing the thickness dependence for the island separations *"d"* (Equation (4)), in the expression for the tunnel resistance, in Equation (1):

$$R(h) = D(C_1 e^{C_3 h^{\frac{2}{3}}} - C_2 h^{\frac{1}{z}})^2 e^{E(C_1 e^{C_3 h^{\frac{2}{3}}} - C_2 h^{\frac{1}{z}})} \quad (6)$$

Fig. 3a shows the resistance as a function of thickness of two copper samples (blue squares and red circles for samples S1 and S2 respectively), which present different slopes for the resistance decay. Through Equation (6), theoretical predictions for the thickness dependence of the resistance were computed. Table 1 shows the values of the parameters used to compute the R in Equation (6).

The values explored for C_1, C_2, C_3 and z (structural parameters) were determined considering the size of the structures that compose the film. Fig. 3b shows a representative AFM image (contact mode) of a 4 nm thick copper sample (*ex situ* characterization). The areas of different island were measured and its mean value (averaged over approximately 200 measurements), was associated to a round island of radius ~27 nm. Based on this value, structural parameters were estimated in order to predict the average island radii in a range between ~10 nm and ~30 nm, as the thickness of the film was increased from 1.5 to 4.5 nm (Fig. 2a).

Table 1
Parameters used in the theoretical prediction computed by Equation (6) showed in Fig. 2.

Sample/ Prediction	C_1 (nm)	C_2 (nm)	C_3 (nm$^{3/2}$)	z	D (Ω/nm^2)	E (nm^{-1})
S1/I	12	6	0.265	1.15	7.0×10^2	1.8
S2/I	12	6	0.30	1.15	5.0×10^1	1.8
S2/II	12	6	0.30	1.2	8.0×10^{-2}	2.5
S2/III	25	9	0.15	1.2	2.6×10^4	0.5

Whereas, different values for C_1, C_2, and C_3 chosen to form a particular set, can produce good fits to experimental data, that freedom is not possible in the case of z. The best predictions were always found for z ~1.2. In previous works, this value for the dynamic scaling exponent has been associated, through Kardar-Parisi-Zhang equation for

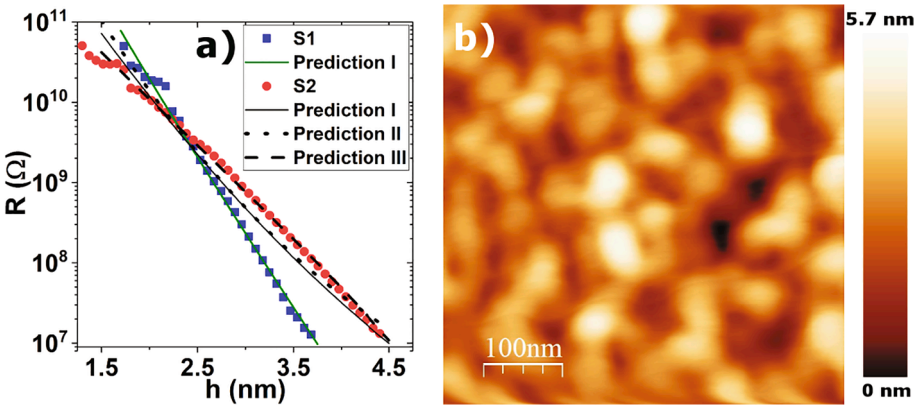

Fig. 3. a) Thickness dependence of the resistance for two copper films and their theoretical predictions generated by Equation 8. b) AFM image (contact mode) of a 4 nm thick copper sample (size 500 × 500 nm^2).

nonconservative and nonequilibrium system [35], to the growth of two-dimensional structures. In this case, the growth process is mainly controlled by atoms arriving to the surface and their subsequent surface diffusion on the substrate. Also, different values for this exponent have been reported depending on the stage of growth. Values between 3 and 4 have been informed togethers with others close to 1, as the film's isolated islands start to coalesce [36,37]. In this sense, the values found for z (Table 1) and the AFM images are consistent with a film in which the islands are coalescing.

On the other hand, the remaining parameters D and E (tunnel parameters) were varied as follows. Whereas D was used as a normalization parameter, the range of values explored for E (also known as tunnel decay constant) was between 0.5 and 4 nm^{-1}, in accord with values reported for similar systems: between 3 and 4 nm^{-1} for Au on Glass [26], and ~2 nm^{-1} for Ag on glass [26]. Our values for E are always closer to those determined for silver than for gold, however in samples as S2 (higher slopes), the best predictions are always reached for $E < 1$. Similar values have been determined for the electrical conduction in saturated n-alkanes [38].

Although many considerations can be made to improve the selection of the adjustable parameters together with the performance of this simple theoretical model, it is remarkable the reasonably good agreement of its predictions. It allows to relate the film structure, characterized by the island's radii and distances, with electrical transport mediated by tunnel current.

Once sample fabrication is completed, the aging process begins. Fig. 4a shows the behavior of the copper film resistance for various films during the first 30 min. All copper samples display a similar time dependence. Resistance keeps increasing without showing a saturation value. Fig. 4 allows the comparison of the time evolution of copper films with those shown by gold and chromium. Whereas gold films present a similar behavior to that of copper samples, chromium layers show a very different trend. In the case of chromium, the resistance, for seemingly identical films, can either increase or decrease without any relation to the experimental preparation conditions. A resistance decrease in system in the vicinity of percolation, has been reported for bismuth nanocluster film. It has been associated to an increase in the neck radius that joins two nanoclusters. In a similar way, a process that improves the contacts between conductive zones of chromium should produce a drop in resistance [39]. However, to our knowledge, this behavior in chromium films has not been previously reported.

For further insight on what causes the resistance increment during aging, one of the gold samples was annealed at 80 °C for 30 min after fabrication. A dashed line was used to indicate R(t) in Fig. 4b. The temperature increase in this case induces a larger change in the film resistance. A similar conclusion was previously reported by Henriquez *et al* [8], but in samples where the percolation was already achieved. The resistance increase of copper and gold ultra-thin films during aging is mainly induced by material diffusion [8,27,29]. Thus, a larger effect on the resistance is measured when the diffusion coefficient increases, for example by increasing temperature. The similarities between gold and copper resistance behavior indicate that atomic diffusion is the common mechanism that controls the films' aging in both cases.

To compare the resistance increase due to aging between different samples, it is reasonable to define a normalized resistance increase ($R(1800)-R(0))/R(0)$). Fig. 4d shows the normalized resistance increase as a function of $R(0)$ for copper, gold and chromium samples. It includes copper films with resistances below ~1×10^6 Ω In the case of copper films, there is a correlation between the resistance increase and its initial resistance value. Also, the normalized change is similar in gold and copper in the high resistances range. This result points out that when the island's distance is large (high resistance), the effect of surface diffusion is more noticeable, allowing the atoms to rearrange into 3D structures increasing the distance between islands, hence, increasing the film resistance. This behavior is expected when the substrate surface energy is lower than that of the adsorbed material. Namely the system presents Volmer-Weber growth (VW). Precisely, chromium on mica does not grow in this way, so, as expected, the resistance evolves differently in this case (Fig. 3c). In this same direction (high resistance implies a larger change) Andersson [27] reported a similar behavior to that shown in Fig. 4d, for gold films evaporated on glass.

To get further understanding on the effect of aging in these films, a comparison between the theoretical model and experimental data was performed. Again, considering a constant temperature during the aging process, in Equation (1), the product $\frac{R_0}{\varnothing} f\left(\frac{\delta E}{kT}\right)$ is replaced by a single constant. Replacing the expression for the distance (Equation (5)), in that for the tunnel resistance (Equation (1)), the time dependence of the resistance is obtained:

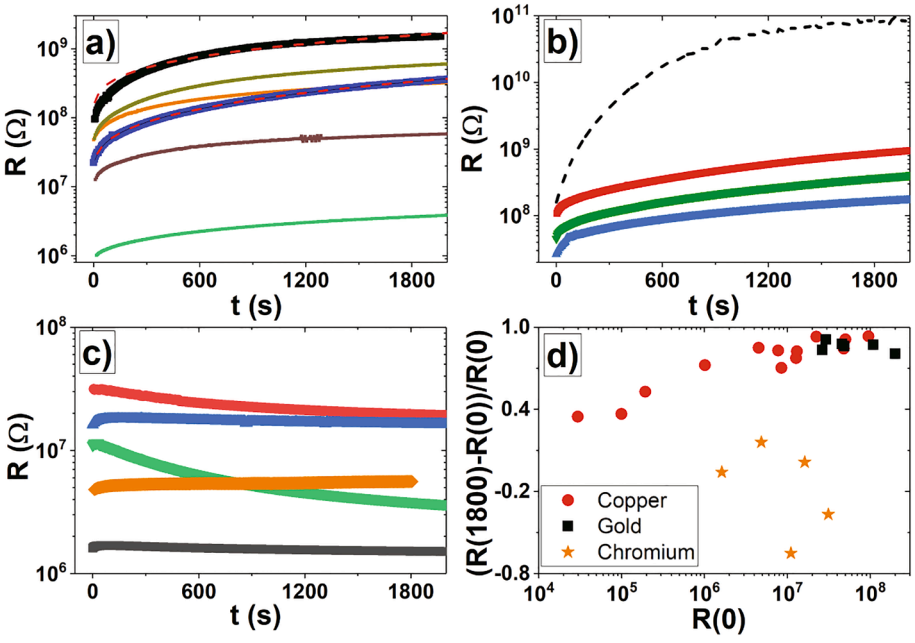

Fig. 4. Time dependence of the resistance during aging for: a) copper, b) gold and c) chromium films. All samples were kept at RT during the measurements, except for the gold trace with a dashed line in Fig. 4b. In the aging of this particular film, the temperature was 80 °C. Dashed lines in Fig. 4a depict the adjusting performed with the Equation (7). d) Normalized resistance increase, $(R(1800)-R(0))/R(0)$ as a function of initial resistance $R(0)$ (resistance at t = 0) for copper (round symbols), gold (square symbols) and chromium (stars) samples.

$$R(t) = D\left(d_0 + D_1\left(\frac{t}{\ln(t)}\right)^{\frac{3}{[2(3+\alpha)]}} - D_1 \cdot D_2\left(\frac{t}{\ln(t)}\right)^{\frac{1}{(3+\alpha)}}\right)^2 \times e^{E\left(d_0 + D_1\left(\frac{t}{\ln(t)}\right)^{3/[2(3+\alpha)]} - D_1 \cdot D_2\left(\frac{t}{\ln(t)}\right)^{1/(3+\alpha)}\right)} \quad (7)$$

For copper samples with an initial resistance, *R(0),* lower than $\sim 5 \times 10^7 \Omega$, the model shows a better fit than for films that exceed this value, independent of other parameters. In Fig. 4a, both behaviors are depicted with dashed lines.

Since the numbers of parameters to determine is large, some way of narrowing the options was introduced. First, based on AFM images (Fig. 3b), an initial separation distance d_0 among islands was selected to be between 3 and 7 nm. Then, choosing $D_1 = 1.2$ and $D_2 = 1.0$, α controls the rate of change of the island distance *d(t)*. Using α, *D* and *E*, as adjustment parameters, the best fit was sought. The best adjustments were found for $3.0 < \alpha < 4.5$ and $0.7\ \text{nm}^{-1} < E < 1.2\ \text{nm}^{-1}$, independent of the value of D. These values of *E*, obtained for the aging process, are in the same range as those used in the previous analysis (see Table 1). The values for α are in good agreement with those obtained from a theoretical model describing the growth of 3D structure by diffusion [29], which predict $\alpha = 3$ for an aging process controlled by volume diffusion of atoms, and $\alpha = 4$, for one dominated by atom diffusion on the substrate. Based on these considerations, our results point out that this last mechanism should be the dominant process in the aging of the films.

As explained in the previous section, the oxidation process was performed in two stages. The "low pressure oxidation" (below 10^3 Pa) and the "high pressure oxidation" (above 10^3 Pa). Fig. 5 shows the evolution of R(t) in copper, gold and chromium samples. Since the effect of the aging is a resistance increase, the last 500 s of this process were added in Fig. 5 to compare the resistance change between aging and the oxidation stages.

Results show that, at the beginning of the low pressure oxidation stage, copper samples' resistance rises as pressure increases, similar to chromium films. However, between the end of low pressure stage and the beginning of high-pressure stage, there is a high instability in the signal, followed by a resistance decay towards a new stable value. This behavior is present in all copper samples, where the resistance at the beginning of the oxidation process is higher than $\sim 3 \times 10^7 \Omega$. In chromium films, this resistance reduction is not observed. On the other hand, gold only shows a slight change for $P > 10^3$ Pa.

To get a better understanding of the resistance change during low pressure oxidation, a normalized resistance change (ΔR/R) was defined for each pressure step, as the difference between the final and the initial resistance, divided by the initial resistance. Fig. 6 shows the pressure dependence of ΔR/R, for copper and chromium films.

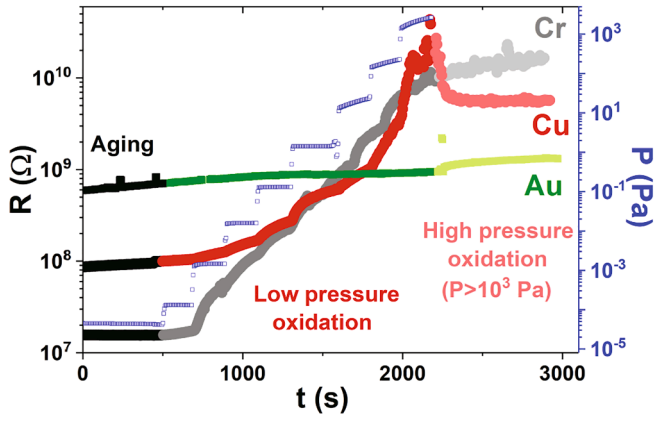

Fig. 5. Effect of the oxidation process on the resistance for chromium, copper and gold films. In all curves three ranges are highlighted with different color shades, they are: the final part of the aging process, low pressure oxidation and high pressure oxidation. Hollow symbols and the right axis represent the pressure steps.

At the beginning of the oxidation process, the resistance change in copper films does not present differences between the effect of aging and the oxidation. At 10^{-3} Pa, a steady increase in ΔR/R was measured. As expected, this increment cannot be reversed by a decrease in pressure (not shown explicitly in the data). About 10^0 Pa, an increase in this change is detected, followed by the appearance of an instability in the electrical signals, and a subsequent resistance decrease. This abrupt change occurs between 10^1 and 10^3 Pa, depending on the sample (negative values in Fig. 6a). A different behavior is observed for chromium samples, showing changes in ΔR/R at pressures as low as 10^{-4} Pa. Also, the maximum value in ΔR/R is reached between 10^{-3} and 10^{-2}Pa. Regarding gold films, all resistance changes are lower than 0.01 at the low-pressure oxidation step, being indistinguishable from the increase due to the aging effects. Only, above 10^3 Pa, a slight increase in ΔR/R is observed, possibly due to the adsorption of molecular species present in air [40]. This change appears clearly displayed in Fig. 5.

To understand, the phenomenon of the resistance decay of the copper samples, two characterizations were performed immediately after the films were oxidized in ambient conditions. For some samples, including some gold and chromium films, the temperature dependence of the resistance was determined. For a second group, Raman spectrometry was performed, with the idea of detecting an oxide derived peak.

Fig. 7a shows the characteristic temperature dependence of the conductance as a function of 1000/(kT) for copper, chromium and gold films. Even though, these samples present almost the same conductance at RT ($\sim 1.4 \times 10^{-9} \Omega^{-1}$), their behavior is very different as the temperature drops. The copper sample presents two different slopes. The first of them, for 200 K < T < 300 K, correspond to a $\delta E = 38$ meV, similar to chromium films with $\delta E = 11$ meV, in this temperature range. The copper film has a different$\delta E = 1.9$ meV for 30 K < T < 150 K, a value similar to that of gold films ($\delta E = 2.3$ meV). To understand the difference between the conduction through islands of gold and a copper in a film, the effect of Cu_2O should be included in the model. Fig. 7b shows a Raman spectrum of a copper thin film fabricated and oxidized under the same conditions as those used in this work. The arrows mark the peaks at 110, 150 and 220 cm^{-1} corresponding to the E_u, T_{1u} and $2E_u$ modes of Cu_2O [41,42]. On the other hand, mica (the substrate) presents a series of strong peaks in this low frequency shifts, making less noticeable the contribution of the cuprous oxide. However, the peak located in 150 cm^{-1} (highlighted with a dashed line in Fig. 7b) overcomes the substrate signal, confirming the presence of Cu_2O in our copper ultra-thin films.

The two-slopes in the conductance vs temperature indicates electronic transport is mediated by two mechanisms. Fig. 7c depicts the formation of a sample with two conduction channels. The copper film presents tunnel conduction similar to that shown by gold islands, however, as copper oxidizes, the Cu_2O covered islands get closer to each other, simply because cuprous oxide has a lower density than copper, hence, a larger volume. Once, Cu_2O islands are close enough, a second conduction channel appears: through cuprous oxide, a semiconductor.

The electrical conduction in these oxidized copper samples, can be represented by the effect of two mechanisms connected as two parallel resistors with different temperature dependences and activation energies. That is:

$$\sigma_{Sample}(T) = \sigma_{Cu}(T) + \sigma_{Cu_2O}(T)$$

where $\sigma_{Cu}(T)$ represents the tunnel conduction through copper islands and, $\sigma_{Cu_2O}(T)$, the semiconductor-type conduction through cuprous oxide. At high temperature (T > 200 K), the predominant mode is that semiconductor-type, whereas at low temperature (T < 150 K), this mechanism decreases its efficiency, dominating the tunnel conduction.

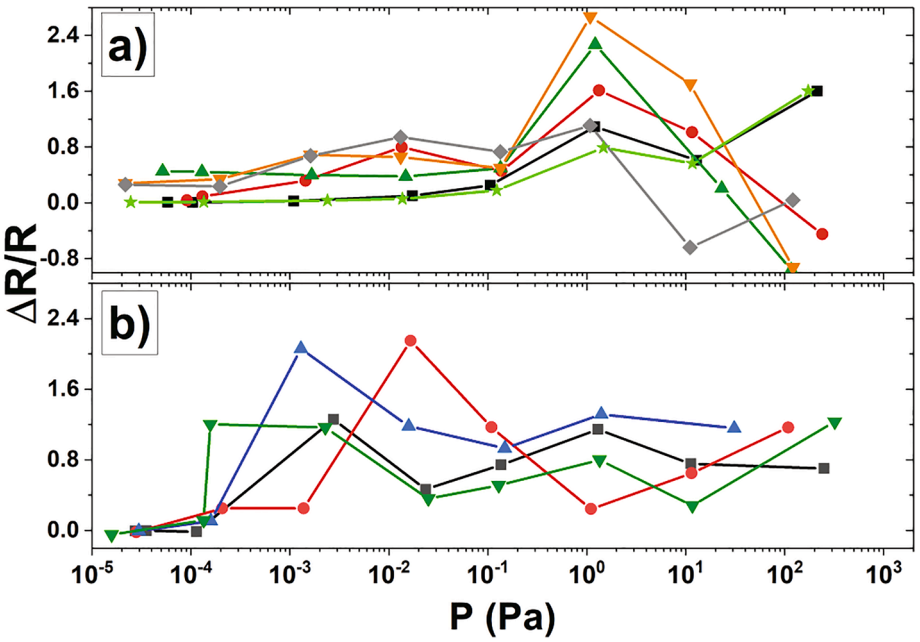

Fig. 6. Normalized resistance change as a function of pressure for a) copper and b) chromium films during the low-pressure oxidation stage.

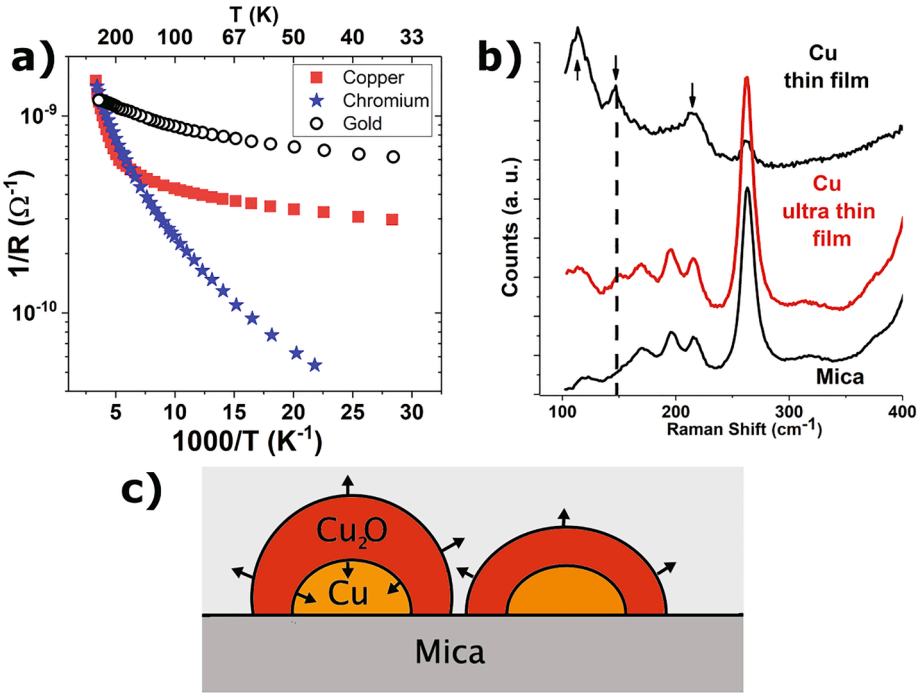

Fig. 7. a) Conductance "1/R" as a function of 1000/T for copper (square symbols), chromium (stars) and gold (round symbols) samples. b) Representative Raman spectrum of a copper thin film, a copper ultrathin film, and mica. Cu_2O peaks are highlighted with arrows. c) Representation of Cu_2O growth on copper islands.

Summary

The electrical transport mechanism of non-percolated copper ultrathin films was studied. For this purpose, resistance behavior was measured during sample growth, aging and oxidation, and contrasted with a model based on tunnel current and on film's morphology. In addition, the electrical characterization of chromium and gold ultrathin films was performed and compared with that obtained for copper.

During the films' growth, copper, gold and chromium, films' resistance presents an almost constant decay between 10^{10} and 10^{7} Ω, as thickness increases approximately up to 4.5, 7.0 and 0.5 nm, respectively. Electrical resistance's linear decrease of copper films was studied by fitting a tunnel transport model which considered islands' distance as a function of film thickness. Either for fast or slow decay, the dynamic scaling exponent obtained was ~1.2, which indicates a resistance reduction given by coalescing islands.

During aging at high vacuum conditions, the resistance of copper and gold ultrathin films increases without reaching a saturation value after 30 min, with a behavior independent of the material or the initial resistance. On the other hand, chromium layers' resistance presents a very different trend: it can increase or decrease depending on the samples. The theoretical model applied to copper film resistance explains

the increment by further formation of 3D structures, mainly conducted by atom diffusion on the substrate. This result is in good agreement with that previously reported for gold films. Since chromium films have a different growth mode, their resistance does not present this behavior during aging.

At the beginning of the oxidation process, under low pressure $\sim 10^{-3}$Pa, the increment in the electrical resistance of chromium films is higher than that observed in copper samples. However, when oxidation pressure reaches 1 Pa, copper films' resistance presents similar changes to those measured in chromium layers. At pressures above ~10 Pa, copper samples show an unstable electrical signal, followed by a noticeable resistance reduction. In these samples, the presence of Cu_2O generates a second electrical transport mechanism, evidenced by the temperature dependence of the film resistance. The electrical conduction is mediated by two contributions, a semi-conductor type resembling that of oxidized chromium layers and a tunnel conduction type observed for gold ultrathin films. The first mechanism dominates when temperature is above 200 K, while tunneling is the main process for temperatures below 150 K.

CRediT authorship contribution statement

Francisca Marín: Formal analysis, Investigation, Methodology. **Gabriel Gray:** Formal analysis, Investigation, Methodology. **Claudio Gonzalez-Fuentes:** Writing - review & editing, Conceptualization, Investigation, Formal analysis, Methodology, Software. **Valeria del Campo:** Writing - original draft, Funding acquisition, Resources, Supervision, Validation. **Patricio Häberle:** Writing - original draft, Funding acquisition, Resources, Supervision, Validation. **Ricardo Henríquez:** Writing - original draft, Conceptualization, Investigation, Formal analysis, Funding acquisition, Supervision, Validation, Project administration.

Declaration of Competing Interest

The authors declare that they have no known competing financial interests or personal relationships that could have appeared to influence the work reported in this paper.

Acknowledgement

RH recognizes Professor Luis Moraga Jaramillo (now deceased) for his enlightening discussions on the subjects related to this article. This work was funded by project "Fondecyt 1181905". F.M. and G.G. acknowledge support from "Programa Incentivo a la Iniciación Científica 2019-USM". R.H and V.d.C acknowledge support from DGIIE-USM grant # PI-LIR-2020-16.

References

[1] Gall D. The search for the most conductive metal for narrow interconnect lines. J Appl Phys 2020;127:050901. https://doi.org/10.1063/1.5133671.
[2] Munoz RC, Arenas C. Size effects and charge transport in metals: Quantum theory of the resistivity of nanometric metallic structures arising from electron scattering by grain boundaries and by rough surfaces. Appl Phys Rev 2017;4:011102. https://doi.org/10.1063/1.4974032.
[3] Henriquez R, Roco R, Bravo S, Del Campo V, Gonzalez-Fuentes C, Donoso S, Häberle P. Effect of a metallic surfactant on the electrical percolation of gold films. Appl Surf Sci 2019;489:403–8. https://doi.org/10.1016/j.apsusc.2019.05.347.
[4] Moraga L, Arenas C, Henriquez R, Bravo S, Solis B. The electrical conductivity of polycrystalline metallic films. Physica B 2016;499:17–23. https://doi.org/10.1016/j.physb.2016.07.001.
[5] Moraga L, Arenas C, Henriquez R, Solis B. The effect of surface roughness and grain-boundary scattering on the electrical conductivity of thin metallic wires: The effect of surface roughness on conductivity of thin metallic wires. Phys Status Solidi B 2015;252(1):219–29. https://doi.org/10.1002/pssb.201451202.
[6] Josell D, Brongersma SH, Tőkei Z. Size-Dependent Resistivity in Nanoscale Interconnects. Annu Rev Mater Res 2009;39:231–54. https://doi.org/10.1146/annurev-matsci-082908-145415.
[7] Andersson T. The electrical properties of ultrathin gold films during and after their growth on glass. J Phys D: Appl Phys 1976;9:973. https://doi.org/10.1088/0022-3727/9/6/010.
[8] Henriquez R, Bravo S, Roco R, Del Campo V, Kroeger D, Häberle P. Electrical Percolation and Aging of Gold Films. Metall and Mat Trans A 2019;50:493–503. https://doi.org/10.1007/s11661-018-4979-3.
[9] Yajadda MMA, Müller K-H, Ostrikov K. Effect of Coulomb blockade, gold resistance, and thermal expansion on the electrical resistance of ultrathin gold films. Phys Rev B 2011;84:235431. https://doi.org/10.1103/PhysRevB.84.235431.
[10] Lassesson A, Brown SA, van Lith J, Schulze M. Electrical characterization of gold island films: A route to control of nanoparticle deposition. Appl Phys Lett 2008;93:203111. https://doi.org/10.1063/1.3027463.
[11] Rycroft IM, Evans BL. The in situ characterization of metal film resistance during deposition. Thin Solid Films 1996;290-291:283–8. https://doi.org/10.1016/S0040-6090(96)09181-X.
[12] Penza M, Rossi R, Alvisi M, Cassano G, Serra E. Functional characterization of carbon nanotube networked films functionalized with tuned loading of Au nanoclusters for gas sensing applications. Sens Actuators, B 2009;140:176–84. https://doi.org/10.1016/j.snb.2009.04.008.
[13] Segura RA, Contreras C, Henriquez R, Häberle P, Acuña JJS, Adrian A, Alvarez P, Hevia SA. Gold nanoparticles grown inside carbon nanotubes: synthesis and electrical transport measurements. Nanoscale Res Lett 2014;9. https://doi.org/10.1186/1556-276X-9-207.
[14] Im JS, Kang SC, Lee S-H, Lee Y-S. Improved gas sensing of electrospun carbon fibers based on pore structure, conductivity and surface modification. Carbon 2010;48:2573–81. https://doi.org/10.1016/j.carbon.2010.03.045.
[15] Bastatas LD, Echeverria-Mora E, Wagle P, Mainali P, Austin A, McIlroy DN. Emergent Electrical Properties of Ensembles of 1D Nanostructures and Their Impact on Room Temperature Electrical Sensing of Ammonium Nitrate Vapor. ACS Sens 2018;3:2367–74. https://doi.org/10.1021/acssensors.8b00746.
[16] Barmak K, Ezzat S, Gusley R, Jog A, Kerdsongpanya S, Khaniya A, Milosevic E, Richardson W, Sentosun K, Zangiabadi A, Gall D, Kaden WE, Mucciolo ER, Schelling PK, West AC, Coffey KR. Epitaxial metals for interconnects beyond Cu. J Vac Sci Technol, A 2020;38(3):033406. https://doi.org/10.1116/6.0000018.
[17] Flores M, Donoso S, Ortiz M, Acosta G, Fernández H. Alkanethiol self-assembled monolayer on copper polycrystalline thin films: Influence on resistivity. Mater Chem Phys 2018;208:97–102. https://doi.org/10.1016/j.matchemphys.2018.01.034.
[18] Platzman I, Brener R, Haick H, Tannenbaum R. Oxidation of Polycrystalline Copper Thin Films at Ambient Conditions. J Phys Chem C 2008;112:1101–8. https://doi.org/10.1021/jp076981k.
[19] Papadimitropoulos G, Vourdas N, Vamvakas VE, Davazoglou D. Deposition and characterization of copper oxide thin films. J Phys: Conf Ser 2005;10:182–5. https://doi.org/10.1088/1742-6596/10/1/045.
[20] Ramanandan GKP, Ramakrishnan G, Planken PCM. Oxidation kinetics of nanoscale copper films studied by terahertz transmission spectroscopy. J Appl Phys 2012;111:123517. https://doi.org/10.1063/1.4729808.
[21] Gattinoni C, Michaelides A. Atomistic details of oxide surfaces and surface oxidation: the example of copper and its oxides. Surf Sci Rep 2015;70:424–47. https://doi.org/10.1016/j.surfrep.2015.07.001.
[22] Chawla JS, Zahid F, Guo H, Gall D. Effect of O2 adsorption on electron scattering at Cu(001) surfaces. Appl Phys Lett 2010;97:132106. https://doi.org/10.1063/1.3489357.
[23] Zheng PY, Deng RP, Gall D. Ni doping on Cu surfaces: Reduced copper resistivity. Appl Phys Lett 2014;105:131603. https://doi.org/10.1063/1.4897009.
[24] Rauh M, Finzel H-U, Wißmann P. The Oxidation Kinetics of Thin Copper Films Studied by Resistivity Measurements. Z Naturforsch 1999;54:117–23. https://doi.org/10.1515/zna-1999-0205.
[25] Horcas I, Fernandez R, Gomez-Rodriguez JM, Colchero J, Gomez-Herrero J, Baro AM. WSXM: A software for scanning probe microscopy and a tool for nanotechnology. Rev Sci Instrum 2007;78:013705. https://doi.org/10.1063/1.2432410.
[26] Hill RM. Electrical conduction in ultrathin metal films. Proc RSoc A 309 1969;377. https://doi.org/10.1098/rspa.1969.0048.
[27] Andersson T. Resistance variation and field effects in thin gold films after growth in an electric field. J Appl Phys 1976;47:1752–6. https://doi.org/10.1063/1.322886.
[28] Ruffino F, Torrisi V, Marletta G, Grimaldi MG. Kinetic growth mechanisms of sputter-deposited Au films on mica: from nanoclusters to nanostructured microclusters. Appl Phys A 2010;100(1):7–13. https://doi.org/10.1007/s00339-010-5797-7.
[29] El-Barraj A, Curiotto S, Cheynis F, Müller P, Leroy F. Dynamics of Au-Ge liquid droplets on Ge(1 1 1) terraces: Nucleation, growth and dynamic coalescence. Appl Surf Sci 2020;509:144667. https://doi.org/10.1016/j.apsusc.2019.144667.
[30] Ruffino F, Grimaldi MG. Island-to-percolation transition during the room-temperature growth of sputtered nanoscale Pd films on hexagonal SiC. J Appl Phys 2010;107(7):074301. https://doi.org/10.1063/1.3361321.
[31] Müller K-H, Herrmann J, Raguse B, Baxter G, Reda T. Percolation model for electron conduction in films of metal nanoparticles linked by organic molecules. Phys Rev B 2002;66. https://doi.org/10.1103/PhysRevB.66.075417.
[32] So SK, Fong HH, Yeung CF, Cheung NH. Transmittance and resistivity of semicontinuous copper films prepared by pulsed-laser deposition. Appl Phys Lett 2000;77:1099–101. https://doi.org/10.1063/1.1289259.
[33] Gladskikh IA, Gushchin MG, Vartanyan TA. Resistance Switching in Ag, Au, and Cu Films at the Percolation Threshold. Semiconductors 2018;52:671–4. https://doi.org/10.1134/S1063782618050093.

[34] Todeschini M, Bastos da Silva Fanta A, Jensen F, Wagner JB, Han A. Influence of Ti and Cr Adhesion Layers on Ultrathin Au Films. ACS Appl Mater Interfaces 2017;9:37374–85. https://doi.org/10.1021/acsami.7b10136.
[35] Kardar M, Parisi G, Zhang Y-C. Dynamic Scaling of Growing Interfaces. Phys Rev Lett 1986;56:889–92. https://doi.org/10.1103/PhysRevLett.56.889.
[36] Beysens D, Knobler CM, Schaffar H. Scaling in the growth of aggregates on a surface. Phys Rev B 1990;41:9814–8. https://doi.org/10.1103/PhysRevB.41.9814.
[37] Gautier-Soyer M, Gota S, Douillard L, Duraud JP, Le Fèvre P. Submonolayer scaling due to coalescence of subnanometric copper clusters on alumina. Phys Rev B 1996;54:10366–9. https://doi.org/10.1103/PhysRevB.54.10366.
[38] Wang Y-H, Hong Z-W, Sun Y-Y, Li D-F, Han Di, Zheng J-F, Niu Z-J, Zhou X-S. Tunneling Decay Constant of Alkanedicarboxylic Acids: Different Dependence on the Metal Electrodes between Air and Electrochemistry. J Phys Chem C 2014;118:18756–61. https://doi.org/10.1021/jp505374v.
[39] Convers PY, McCarthy DN, Sattar A, Natali F, Hendy SC, Brown SA. Electrical signature of nanoscale coalescence in a percolating Bi nanocluster film. Phys Rev B 2010;82. https://doi.org/10.1103/PhysRevB.82.115409.
[40] Peter Wißmann, Hans-Ulrich Finzel. Electrical Resistivity of Thin Metal Films. Springer Tracts in Modern Physics, Volume 223, Chapter 5 and 6. 2007.
[41] Sander T, Reindl CT, Klar PJ. Breaking of Raman selection rules in Cu 2 O by intrinsic point defects. MRS Proc 2014;1633:81–6. https://doi.org/10.1557/opl.2014.47.
[42] Reimann K, Syassen K. Raman scattering and photoluminescence in Cu2O under hydrostatic pressure. Phys Rev B 1989;39:11113. https://doi.org/10.1103/physrevb.39.11113.